The HKU Scholars Hub   The University of Hong Kong   香港大學學術庫

Title	Mineralization of perfluorooctanesulfonate (PFOS) and perfluorodecanoate (PFDA) from aqueous solution by porous hexagonal boron nitride: adsorption followed by simultaneous thermal decomposition and regeneration
Author(s)	FENG, Y; ZHOU, Y; Lee, P.H.; Shih, K
Citation	RSC Advances, 2016, v. 6, p. 113773-113780
Issued Date	2016
URL	http://hdl.handle.net/10722/246555
Rights	This work is licensed under a Creative Commons Attribution-NonCommercial-NoDerivatives 4.0 International License.

Mineralization of perfluorooctanesulfonate (PFOS) and perfluorodecanoate (PFDA) from aqueous solution by porous hexagonal boron nitride: adsorption followed by simultaneous thermal decomposition and regeneration†

Yong Feng,[a] Ying Zhou,[a] Po-Heng Lee[b] and Kaimin Shih*[a]

Poly- and perfluoroalkyl substances (PFASs) are of global concern due to their toxicity, high persistency, bioaccumulation, and worldwide occurrence. Boron nitride (BN), consisting of light elements and bearing excellent thermal stability, has shown great potential in wastewater purification as a readily-recyclable sorbent. In this study, porous hexagonal BN nanosheets (h-BNs) were synthesized and for the first time their sorption capacities toward perfluorooctanesulfonate (PFOS) and perfluorodecanoate (PFDA) (two representative PFASs) were evaluated under various solution compositions. The h-BNs used after sorption were regenerated by calcining at 600 °C in air for 20 min. The h-BNs synthesized were found to have fast sorption kinetics for both PFOS and PFDA, and the sorption processes fitted well with the Freundlich model and pseudo-second-order kinetics. Under the conditions of 50 mg L^{-1} PFDA or PFOS, 0.2 g L^{-1} h-BNs, and pH 6.0, sorption capacities of $\sim$0.72 mg m^{-2} and $\sim$0.45 mg m^{-2} were achieved for PFDA and PFOS, respectively. The effects of H$^+$ and Ca^{2+} showed that electrostatic interactions were responsible for the sorption. The reutilization experiments revealed that the h-BNs had a persistent sorption capacity after three cycles. To reduce the production of fluorine-containing gases, calcium hydroxide was used as a calcination additive and the fluorine-fixing product calcium fluoride was successfully detected. The results suggest that h-BN sorption may be a promising approach for the removal of PFASs from an aqueous solution.

1. Introduction

Poly- and perfluoroalkyl substances (PFASs), particularly subsets of perfluoroalkyl sulfonates (PFSAs) and perfluoroalkyl carboxylates (PFCAs), have been widely used in industries such as metal plating, aqueous film forming foams, and polymerization, due to their ability to lower surface tension, their superior stability under chemical erosion, and their ability to create foams.[1–3] However, widespread use has resulted in ubiquitous distribution of these compounds in water bodies,[4,5] sediments,[6] wildlife,[7] and humans.[8,9] Due to their toxicity, high persistency, and bioaccumulation, some PFASs are considered as contaminants causing global concern.[10] Perfluorooctanesulfonate (PFOS; C$_8$F$_{17}$SO$_3^-$, Table S1†), one of the most intensively used perfluoroalkyl sulfonates, is almost naturally un-degradable and has been listed as a persistent organic pollutant under the Stockholm Convention since 2009. A study on PFOS in polar bears showed that this compound has an even higher bioaccumulation than polychlorinated biphenyls.[11] The production and use of this substance has been restricted since 2009, but PFOS is still the PFAS most often found at the highest level in the environment,[12,13] probably due to its past releases, generation from precursors, and exemption from phase-out in certain applications. Paul et al.[2] estimated that around 122 500 tons of perfluorooctane sulfonyl fluoride, a major precursor of PFOS, was produced from 1972 to 2000, resulting in the release of 450 to 2700 tons of PFOS into wastewater. Perfluorodecanoic acid (PFDA; C$_{10}$HF$_{19}$O$_2$, Table S1†), a long-chain perfluoroalkyl carboxylate similar to perfluorooctanoate (PFOA; C$_8$HF$_{15}$O$_2$), is commonly used as a surfactant and emulsifier in the fluoropolymer industry and in aqueous film forming foams.[3] Our previous study showed that PFDA widely occurs in the sludge from drinking water and wastewater treatment plants.[6] Its concentration is significantly lower than that of PFOS, but is comparable with the level of PFOA. Similar results were also reported in the inventory survey of Venkatesan et al.,[14] who found that there was $\sim$26 ng of PFDA per gram of bio-solids, just slightly lower than the average value of PFOA (34 ng g^{-1}). The toxicity and occurrence of PFDA has

[a]Department of Civil Engineering, The University of Hong Kong, Pokfulam Road, Hong Kong, China. E-mail: kshih@hku.hk; Fax: +852-2559-5337; Tel: +852-2859-1973

[b]Department of Civil and Environmental Engineering, The Hong Kong Polytechnic University, Hung Hom, Hong Kong, China

† Electronic supplementary information (ESI) available. See DOI: 10.1039/c6ra15564b

been widely reported over the past decade,[10,15,16] but knowledge of the fate and transport of PFDA is limited.

PFOS is extremely persistent, so conventional methods such as activated sludge processes are almost entirely ineffective for the degradation of this compound. Even Fenton reagents relying on hydroxyl radicals, one of the most powerful advanced oxidation technologies, are found to be almost inert toward PFOS. External-energy assisted approaches such as photolysis or photocatalytic degradation,[17–19] thermal or photo-assisted persulfate oxidation,[20,21] sonochemical transformation,[22,23] and electrochemical treatment[24,25] are currently the only known methods effective for PFOS degradation.

Sorption is an energy-saving approach for the removal of anionic surfactants from aqueous solution. The sorption of PFOS and PFOA onto many sorbents such as sediments,[26,27] carbon-based materials,[28–30] and minerals[31–33] has been extensively investigated in recent years. Of these, powder activated carbon has the highest sorption capacity. According to Yu et al.,[28] a sorption capacity of ~519.0 mg L^{-1} PFOS per g of activated carbon powder can be realized. However, in spite of the high uptake, a major drawback with these sorption techniques is that no degradation/mineralization of PFOS occurs. The reutilization performance of these sorbents, which is important for preventing probable second pollution and lowing the operating cost, has been rarely reported.

Boron nitride (BN), or "white graphene" has remarkable properties[34] such as a wide bandgap (5.5–6 eV), chemical inertness, and high thermal stability, which are complementary to graphite. Super-stability at high temperatures indicates that BN can easily be thermally regenerated in air, which is a major advantage over other common carbon-based sorbents. In addition, BN with highly porous nano-structures can be synthesized. BN nanosheets with a high specific surface area of up to 2078 m^2 g^{-1} were recently reported by Li et al.[35] These properties make BN an ideal sorbent candidate for water decontamination in various applications, such as oil separation,[36,37] dye removal,[38] and heavy metal separation.[39,40] Sorption capacities up to 33 times the weight of BN for oil and organic solvents have been reported.[41]

In this study, we synthesized porous hexagonal BN nanosheets (h-BNs), and examined for the first time the sorption of PFOS and PFDA onto the h-BNs under various solution compositions. As a comparison, the sorption property of commercial h-BNs (ch-BNs) was also evaluated. Pseudo-second-order kinetics and the Langmuir and Freundlich isotherms were used to model the sorption and calculate the maximum sorption capacities. High-temperature calcination was used to regenerate the h-BNs and decompose PFOS and PFDA simultaneously. Finally, to avoid the production of short-chain fluorinated gases, Ca(OH)$_2$ was used as an additive to fix the fluorine produced during the thermal-induced defluorination process.

2. Materials and methods

2.1. Chemicals

Potassium PFOS (98%), PFDA (98%), ch-BNs (99%), calcium hydroxide (Ca(OH)$_2$, ≥96%), and high-performance liquid chromatography (LC)-grade ammonium acetate (≥99.0%) were obtained from Sigma-Aldrich (St. Louis, MO, USA). Alumina powder (676a) for quantitative analysis was purchased from National institute of standards and technology (Gaithersburg, MD, USA). Optima LC/mass spectrometry (MS)-grade methanol was provided by Fisher Scientific (Pittsburgh, PA, USA). Other chemicals were of ACS reagent grade and were used as received. All solutions were prepared with ultra-pure water (18.0 MΩ cm) drawn from a Barnstead EASYpure UV/UF water purification system (Boston, MA, USA). In the following sections, BN was used to represent both h-BN and ch-BN.

2.2. Synthesis of h-BNs

h-BNs were synthesized with a modified chemical approach as proposed by Nag et al.[42] In a typical procedure, a boric acid and urea mixture with a molar ratio of 1 : 48 was first dissolved in 40 mL ultra-pure water, and heated to 80 °C with stirring to evaporate the water. The dry product obtained was then put into an OTF-1200X horizontal tube furnace (MTI KJ Group, Hefei, China) and calcined at 900 °C for 8 h with a heating rate of 5 °C min^{-1} in a N$_2$ atmosphere to yield a white product (inset, Fig. 2a). Before the sorption test, the product was ground into powder in an agate mortar, washed with pure water, and dried at 105 °C in a Memmert electric oven (Schwabach, Germany).

2.3. Characterization

The X-ray diffraction patterns of BN were analyzed with a Bruker D8-advanced diffractometer (Karlsruhe, Germany) with a Cu X-ray tube. The operating voltage and current were 40 kV and 40 mA, respectively. The quantitative analysis of the mixture after calcination was processed with the TOPAS (version 4.0) crystallographic program. A refinement approach using alumina powders as the internal standard were used to quantify the amorphous content that was supposed to be produced during the calcination process.[43,44] The Brunauer–Emmett–Teller specific surface area and pore size distribution were determined with a Micromeritics 3Flex surface analyzer (Norcross, GA, USA). The morphology of BN was observed with a Hitachi S-4800 field emission scanning electron microscopy (Tokyo, Japan), a FEI Tecnai G2 20 scanning transmission electron microscope (Hillsboro, OR, USA), and a Nanoscope III Multimode atomic force microscopy (Bruker AXS, Karlsruhe, Germany). The Fourier transform infrared spectroscopy spectra of h-BNs and their precursor were recorded on a Nicolet Magna-IR 750 spectrometer (Waltham, MA, USA). To determine the decomposition temperature of PFOS and PFDA, the pure chemicals were analyzed with a SDT-Q600 thermogravimetry (TG) analyzer (TA instruments, New Castle, DE, USA) in air atmosphere. The isoelectric point of the sample was determined with a Coulter Delsa 440SX zeta potential analyzer (Beckman, Fullerton, CA, USA).

2.4. Sorption experiments

Unless otherwise specified, all experiments were carried out in 50 mL polypropylene copolymer Nalgene centrifuge tubes (Rochester, NY, USA), which we previously found to be the best reactors for PFAS study.[45] First, 20 mL PFDA or PFOS solutions (0.4–50 mg L^{-1}) containing 5 mM ammonium acetate with

certain pH value were added to the tubes, followed by the introduction of 0.004 g h-BNs or 0.02 g ch-BNs to initiate the sorption. To investigate the effect of H^+, the pH value of PFAS solutions was adjusted with 0.1 M NaOH or 0.1 M $HClO_4$ and no buffer was used; to explore the effects of Ca^{2+}, specified volumes of $CaCl_2$ solution were added to the PFAS solution containing 5 mM ammonium acetate before introducing BNs. The tube reactors were then placed on a Lab-line orbital shaker (Wazobia Enterprise, Missouri City, Texas, USA) at 150 rpm at 23 ± 2 °C, controlled by a LMS Series 1A cooled incubator (Sevenoaks, UK). The reactors were sacrificial and duplicate tubes were sampled at each time point. The h-BNs containing PFAS were regenerated by calcining the mixtures at 600 °C in air for 20 min. The calcination temperature was based on the TG results of both PFOS and PFDA (Fig. 6c). The equilibrium sorption capacity of the PFASs was calculated with the following equation:

$$q_e = \frac{(C_0 - C_e) \times V \times S}{1000 \times M} \tag{1}$$

where q_e is the equilibrium sorption amount (mg m^{-2}), C_0 is the initial concentration of PFAS (mg L^{-1}), C_e is the equilibrium concentration (mg L^{-1}), V is the volume of PFAS solution (mL), S is the specific surface area of the sorbent (m^2 g^{-1}), and M is the weight of the sorbent (g).

2.5. Statistical analysis, models, and isotherms

A one-way analysis of variance based on F distribution was used to test whether there was significant difference between the sorption of PFDA and PFOS on to BN. The test was carried out with OriginPro 8 Statistics (v8.0951).

The pseudo-second-order model, which can be expressed by eqn (2), has been widely used to describe pollutant removal in aqueous interfacial reactions.[28,46]

$$\frac{t}{q_t} = \frac{1}{k_2 q_e^2} + \frac{t}{q_e} \tag{2}$$

where t is the reaction time (h), q_t is the amount of sorbate on the surface of h-BNs (mg m^{-2}), q_e is the amount of sorbate adsorbed at the equilibrium (mg m^{-2}), and k_2 is the rate constant of second-order sorption (m^2 mg^{-1} h^{-1}).

To evaluate the equilibrium conditions, the commonly used Langmuir and Freundlich isotherms were used to model the sorption of PFAS onto the h-BNs. These are expressed by eqn (3) and (4), respectively.

$$q_e = \frac{b q_m C_e}{1 + b C_e} \tag{3}$$

$$q_e = K_F C_e^{n-1} \tag{4}$$

where q_m (mg m^{-2}) is the maximum sorption capacity; q_e (mg m^{-2}) is the amount of sorbate on the surface of h-BNs at equilibrium; C_e (mg L^{-1}) is the equilibrium concentration; b (L mg^{-1}) and K_F ((mg m^{-2}) (mg L^{-1})$^{-n}$) are the constants representing sorption equilibrium and sorption capacity, respectively; n^{-1} represents the nonlinearity (n^{-1} for a linear isotherm).

2.6. Analysis of PFASs

The detailed procedures for the analysis of PFASs can be found in our previous work,[6] but to summarize, after the sorption experiments the tubes were centrifuged at 4000 rpm for 3 min at 10 °C (Centrifuge 5810R, Eppendorf, Germany). 1.0 mL of the supernatant was diluted with 2.4 mL LC/MS-grade methanol, and then filtered with 0.22 μm Whatman inorganic membrane filters (Maidstone, UK). The initial 2 mL filtrates were discarded to reduce the influence of filter interception. The Whatman filters show the lowest sorption toward PFASs.[45] The concentrations of PFOS, PFDA, and short-chain PFASs were analyzed with a Waters Acquity ultra-performance LC (UPLC) system, equipped with a Waters Acquity tandem quadruple mass spectrometer (MS/MS; Milford, MA, USA). The separation was performed on a 50 × 2.1 mm Waters BEH C18 column (1.7 μm particle size) at 50 °C with a VanGuard pre-column (5 mm × 2.1 mm, 1.7 μm). To delay the responses from the solvent contaminants, an external Waters isolator column was used before injection into the UPLC separation column. The detection limits for both PFOS and PFDA were lower than 0.1 μg L^{-1}. The chromatograms of standard PFSAs and PFCAs were shown in Fig. S3.† To minimize any matrix-induced effects, the calibration standards were prepared in a 70 : 30 (v/v) methanol/water solution. To determine if the PFASs remaining in the mixtures calcined, 50 mg of the solid was extracted with 40 mL methanol under sonication (Branson 8200, Danbury, CT, USA) for 20 min at ambient temperature, centrifuged at 4000 rpm for 10 min, and filtered with the Whatman filters before analysis.

3. Results and discussion

3.1. Characterization of h-BNs and ch-BNs

In the Fourier transform infrared spectroscopy spectrum of the sample precursor (Fig. 1a), peaks at ~1453 cm^{-1} and ~1656 cm^{-1} were observed, corresponding to the C–N stretching vibration and C=O stretching mode of urea,[47] respectively. After calcining for 8 h, these two peaks almost disappeared and two new characteristic bands occurred at ~774 cm^{-1} and ~1398 cm^{-1}, which could be assigned to the plane B–N–B bending mode and the in-plane B–N stretching mode, respectively.[48] The X-ray powder diffraction pattern (Fig. 1b) shows that the prepared sample displayed two broad peaks at ~27° and ~42°, corresponding to the lattice (002) and (100) planes of standard hexagonal boron nitride (PDF #73-2095, International Centre for Diffraction Data), which suggests that the h-BNs were successfully synthesized. Using the IUPAC classification, the N_2 sorption isotherm of the sample (Fig. 1c) can be categorized as type III. The specific surface area of the h-BNs was calculated using the Brunauer–Emmett–Teller model and found to be 125.5 m^2 g^{-1}. The pore diameter and pore volume of the sample were determined as 3.8 nm and 0.915 cm^3 g^{-1}, respectively. The zeta potential analysis revealed that its isoelectric point was ~3.8 (Fig. 1d).

The scanning electron microscopy image shows that the as-prepared h-BNs consist of highly porous structures (Fig. 2a). The presence of nitrogen and boron on the h-BN surface was confirmed by the energy-dispersive X-ray spectroscopy spectrum
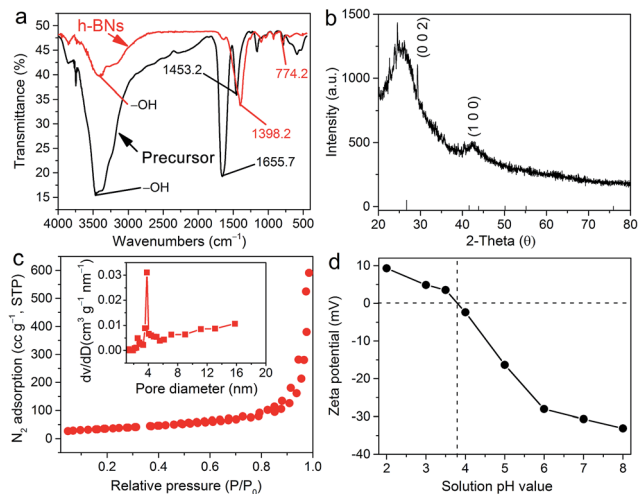
Fig. 1 (a) Fourier transform infrared spectroscopy spectra of h-BNs and their precursor, (b) X-ray powder diffraction pattern and (c) N_2 adsorption–desorption isotherms measured at 77 K of h-BNs, and (d) zeta potential of h-BNs under different solution pH values in the presence of 5 mM ammonium acetate buffer. The inset in (c) shows the pore size distributions from the desorption branches through the Barrett–Joyner–Halenda method.

(Fig. 2b). The transmission electron microscopy image shows that graphene-like few-layer structures are present in the h-BNs (Fig. 2c and d). The interlayer spacing is ~3.2 Å (Fig. 2d), corresponding to the lattice (002) plane of h-BNs. The selected-area electron diffraction pattern (Fig. 2e) shows two diffraction rings of the h-BNs ((110) and (100)). Fig. 2f and e show an atomic force microscopy image and the corresponding height profile of the h-BNs, respectively. An average thickness of ~0.3 nm was observed, which is consistent with the transmission electron microscopy results.

The crystal structure of ch-BNs is hexagonal and the primary powder size ~150 nm, according to the manufacturer's specification and also confirmed by the X-ray diffraction pattern (Fig. S1†) and scanning electron microscopy observations (Fig. S2†). Their specific surface area was determined to be 13.8 $m^2 g^{-1}$.

3.2. Sorption kinetics and isotherms

To determine the time required for equilibrium, the sorption kinetics of both PFDA and PFOS onto the h-BNs and ch-BNs were studied (Fig. 3a and c). Both PFDA and PFOS had fast sorption onto the sorbents. After a contact time of 2 h, ~72% (52%) and ~45% (31%) of PFDA and PFOS were removed, respectively, when h-BNs (ch-BNs) were present as the sorbents. With a further increase of contact time, no obvious differences in the PFAS concentration were observed. Therefore, the reaction time for the sorption study was fixed at 2 h. The fitting results show that the sorption of PFDA and PFOS could be well described by this model, regardless of whether h-BNs or ch-BNs were used. The good fitting coefficients in Fig. 3b and d indicate that the sorption was probably controlled by chemisorption processes and the uptake capacity was proportional to the availability of the active sites on the surface of h-BNs.[49] According to the fitting results, the equilibrium sorption capacities of PFDA and PFOS onto the h-BNs were 0.03 mg m^{-2} and 0.02 mg m^{-2}, respectively, when 1 mg L^{-1} PFAS was present. The relatively higher PFDA sorption amount suggests that this is much more easily adsorbed than PFOS. Generally, PFOS shows higher sorption on sorbents than PFOA due to the sulfonate moiety and longer perfluorinated carbon chain in its structure.[28] The relatively higher removal of PFDA over PFOS, which was tested to be statistically significant ($p = 0.05$), was therefore probably due to the dominant role of the chain-length effect.
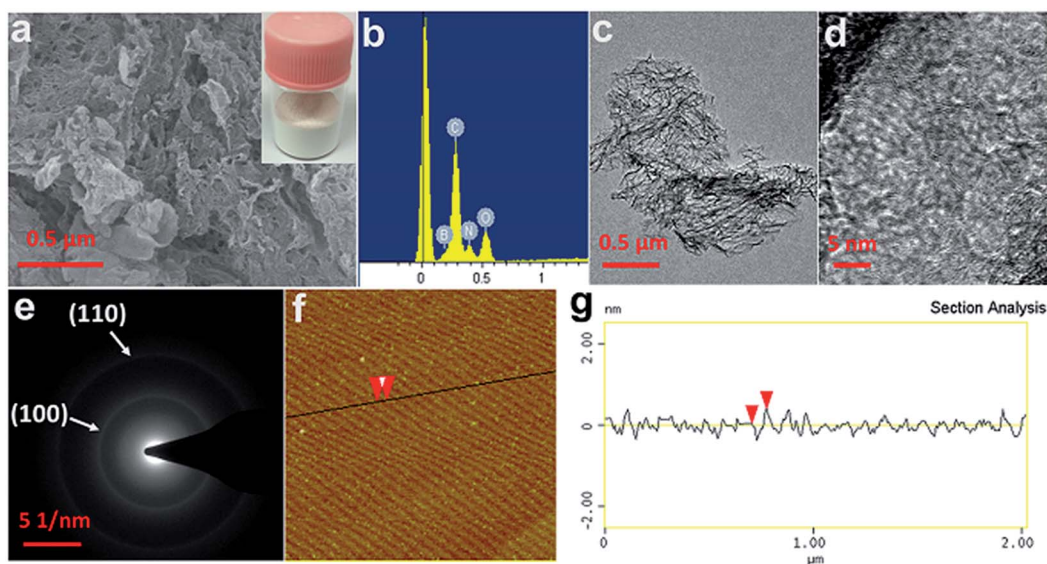

Fig. 2 (a) Scanning electron microscopy, (b) energy-dispersive X-ray spectroscopy, (c) transmission electron microscopy, (d) high-resolution transmission electron microscopy images, (e) diffraction rings of the prepared h-BNs, (f) atomic force microscopy image of h-BNs on mica, and (g) cross section along the black line in (f). The image of h-BNs is shown in the inset in (a).
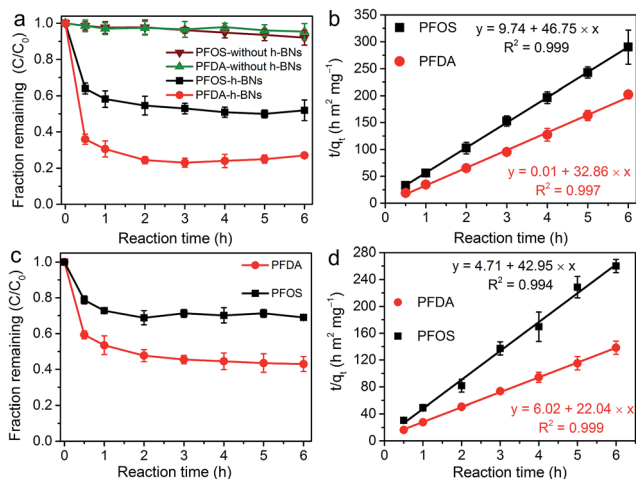
Fig. 3 PFDA and PFOS sorption kinetics onto h-BNs (a) and ch-BNs (c) ([PFDA] = [PFOS] = 1 mg L^{-1}, [h-BNs] = 0.2 g L^{-1}, [ch-BNs] = 1 g L^{-1}, and 5 mM ammonium acetate buffer at pH 6.0); pseudo-second-order kinetic plots of PFASs on h-BNs (b) and ch-BNs (d); the error bars in the figures represent the standard deviation of duplicates; the solid lines in (b) and (d) represent the pseudo-second-order model.

By plotting C_e/q_e *versus* C_e, the q_m and b in the Langmuir model can be calculated. As displayed in Fig. 4a and b and Table 1, the Freundlich isotherm was more appropriate than the Langmuir isotherm in modeling the sorption. The Langmuir isotherm assumes that sorbates are distributed on the sorbent surface in a monolayer manner, whereas the Freundlich isotherm is an empirical model used in nonlinear sorption situations. The Freundlich fitting results demonstrate that the sorption of PFDA (n^{-1} = 0.60) and PFOS (n^{-1} = 0.75) are nonlinear. Nonlinearity typically results from causes such as chemical-specific interactions between the ionic functional group in PFASs and the sorbent, interactions between the ionic functional group in solution and on the sorbent, and solution compositions (*e.g.*, pH conditions and buffer).[26] In the tested pH range the h-BNs were negatively charged (Fig. 1d), so the nonlinearity was probably due to the repulsive force between the negative charged h-BN surface and the deprotonated PFDA or PFOS.
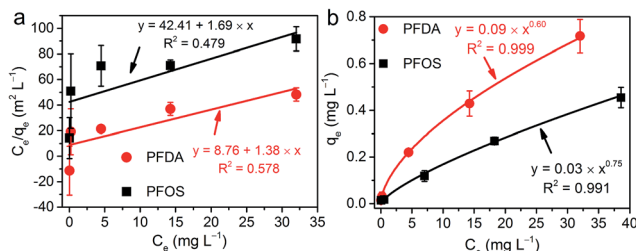

Fig. 4 PFOS and PFDA adsorption isotherms fitted with the Langmuir (a) and Freundlich models (b) when h-BNs were used ([PFDA] = [PFOS] = 0.4–50 mg L^{-1}, [h-BNs] = 0.2 g L^{-1}, and 5 mM ammonium acetate buffer at pH 6.0); the error bars in the figures represent the standard deviation of duplicates; the solid lines in (a) and (b) represent the Langmuir and Freundlich fittings, respectively.

Table 1 Calculated constants of the Langmuir and Freundlich models for the sorption of PFOS and PFDA onto h-BNs

Adsorbate	Langmuir constants			Freundlich constants		
	q_m (mg m^{-2})	b (L mg^{-1})	R^2	K_F (mg m^{-2}) (mg L^{-1})$^{-n}$	n^{-1}	R^2
PFDA	0.16	0.73	0.578	0.09	0.60	0.999
PFOS	0.04	0.60	0.479	0.03	0.75	0.991

Critical micelle concentration (CMC) is an important property of fluorinated surfactants to predict their aqueous behavior. When the PFAS surfactant reaches 0.1 to 1.0% of its CMC, hemi-micelles may form on the sorbent surface.[50] In aqueous solution, CMC is dependent on solution compositions such as surfactant counterions. CMC values of 3992.0 and 462.6 mg L^{-1} were reported for PFOS and PFOA, respectively, when potassium ions are the dominant counterions.[51] When ammonium ions were dominant, the CMC values were expected to be even lower. Formation of hemi-micelle on the h-BN surface is therefore expected, but the formation usually begins with regular sorption at low concentrations, followed by a sharp increase when concentrations reach hemi-micelle levels.[31] In Fig. 4a and b, no such a sharp increase in the sorption can be observed. Therefore, the formation of hemi-micelles may occur, but should not be significant. Under conditions of 50 mg L^{-1} PFAS, 0.2 g L^{-1} h-BNs, and pH 6.0, sorption capacities of ~0.72 mg m^{-2} and ~0.45 mg m^{-2} were achieved for PFDA and PFOS, respectively. This is indicative of a more favorable sorption of PFDA onto the h-BNs than PFOS, in agreement with the pseudo-second order modeling results.

3.3. Effects of solution compositions

Numerous studies have demonstrated the influence of H$^+$ on ionic surfactant sorption. Generally, there are two mechanisms mainly responsible for the H$^+$-dependent sorption:[26] (i) occurrence of specific reactions (*e.g.*, ligand exchange and complexation); (ii) variation of surface charge and protonation/deprotonation of the ionic surfactants. The former is prominent when iron or aluminum-containing sorbents are present. In this study, the concentration of [H$^+$] was controlled by adjusting the pH value of the PFDA or PFOS solutions. Fig. 5a and b show the sorption of PFDA and PFOS onto the h-BNs under different initial solution pHs. As revealed by the regression coefficients, all of these processes were modeled quite well with the Freundlich fitting. It is worth noting that an obvious decrease in both the sorption of PFDA and PFOS was noticed with the increase of solution pH value. In the presence of 5 mM ammonium acetate, the isoelectric point of the h-BNs was estimated to be 3.8 (Fig. 1d); the surface of h-BNs was negatively charged in the pH range of 4.0–10.0. As PFOS and PFDA had pK_a values of −3.27 and 0.52 (Table S1†),[51] respectively, both of these compounds mainly existed as deprotonated (negative) forms when the solution pH value was higher than 4.0. Consequently, electrostatic repulsions rather than attractions occurred between the surface of h-BNs and the two PFASs investigated, which seems inconsistent with the effect of the
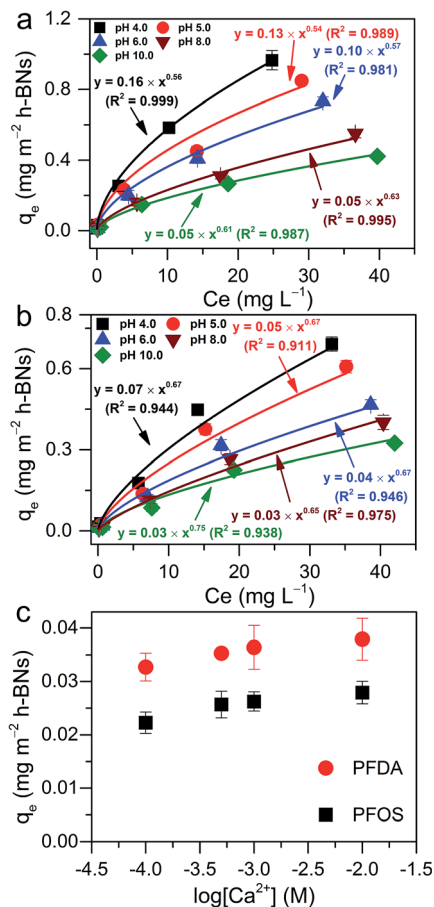
Fig. 5 Effect of solution pH on the sorption of (a) PFDA and (b) PFOS ([h-BNs] = 0.2 g L^{-1} and [PFDA] = [PFOS] = 0.4–50 mg L^{-1}); (c) effect of Ca^{2+} on the sorption of PFDA and PFOS onto h-BNs ([PFDA] = [PFOS] = 1 mg L^{-1}, [h-BNs] = 0.2 g L^{-1}, and 5 mM ammonium acetate buffer at pH 6.0). The error bars in the figures represent the standard deviation of duplicates.

solution pH in Fig. 5a and b. Tang *et al.*[32] examined the sorption of PFOS onto silica and found that the solution pH had a strong influence at an ionic strength of 10 mM NaCl. This pH-dependence observation was related to the significant depression of the electrostatic repulsions, probably caused by the combined effects of low pH conditions and high ionic strength. Similarly, the strong pH-dependent sorption in this study was also probably due to the depression of the electrostatic repulsions.

Fig. 5c shows the sorption of PFDA and PFOS under different levels of Ca^{2+}. An obvious positive correlation between the sorption and Ca^{2+} level could be noticed when log[Ca^{2+}] was increased from −4.0 to −2.0. This phenomenon was consistent with the effects of solution pH reported above and previously,[26,27] where Ca^{2+} also had a significant promotion effect. When Ca^{2+} ions were added to the PFDA or PFOS solution with h-BNs, they may partly neutralize the negative charges on the h-BN surface and thus reduce the electrostatic repulsions between the negatively charged PFASs and the sorbent. Therefore, on the basis of the effects of H$^+$ and Ca^{2+}, it could be concluded that the electrostatic interacts were responsible for the sorption.

3.4. Decomposition and simultaneous regeneration

To further investigate the fate of PFDA and PFOS in the suspensions of h-BNs, the h-BNs used after sorption were extracted with methanol, and the PFDA (PFOS) in the extractions was quantified and compared with those based on the aqueous solution (Fig. 6a and b). Under all pHs tested, the amounts of PFDA and PFOS on the h-BNs generally matched well with their mass loss in aqueous solutions. The slightly lower capacities calculated, based on the extraction method, were probably due to incomplete recollecting of the h-BNs *via* centrifugation.

The TG-DSC curves (Fig. 6c) show that PFOS decomposed at ∼480 °C and PFDA at below 200 °C. To ensure complete and rapid decomposition occurred, the h-BNs were treated with a calcining temperature of 600 °C. The UPLC-MS/MS quantification showed that after calcination, no PFDA and PFOS were present on the h-BNs. No short-chain PFSAs, such as perfluorohexanesulfonate (PFHxS) or perfluorobutanesulfonate (PFBuS), or PFCAs such as perfluorononanoate (PFNA), perfluorooctanoate (PFOA), or perfluoroheptanoate (PFHpA) were detected, indicating the probable complete mineralization of both surfactants. The reutilization experiments (Fig. 6d) showed that the sorption capacity of h-BNs remained nearly constant in the multiple sorption cycles. These observations suggest that the h-BNs had high stability and the thermal regeneration with simultaneous pollutant decomposition was feasible.

3.5. Fluorine fixing with Ca(OH)$_2$

In the calcination process, short-chain fluorinated gases such as CF$_4$ and C$_2$F$_6$ are expected to be produced during the transformation of PFOS or PFDA,[44] and these intermediates are potent greenhouse gases. Identifying the measures to prevent the generation of these fluorine-containing gases is therefore important. In our previous studies Ca(OH)$_2$ was found to be effective in the stabilization of fluoride from the decomposition
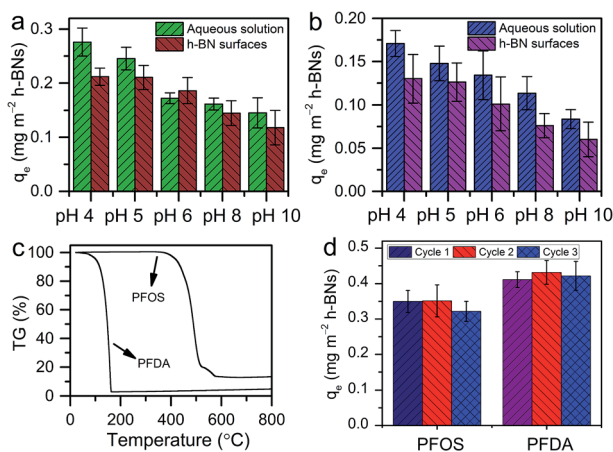

Fig. 6 Amounts of (a) PFDA (a) and (b) PFOS adsorbed quantified from aqueous solution and h-BN surface; (c) TG curves of PFDA and PFOS in air and (d) reusability of h-BNs after calcining at 600 °C for 20 min. The error bars in the figures represent the standard deviation of duplicates.
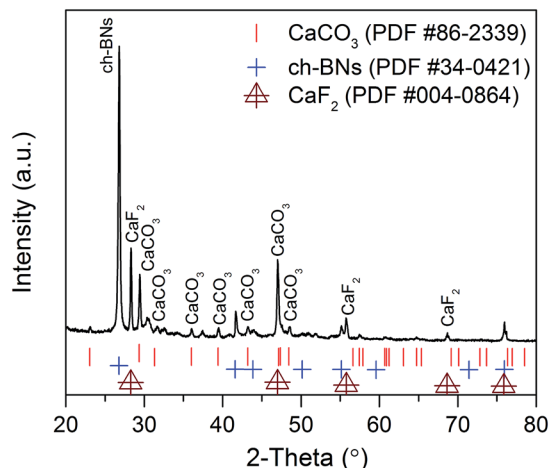
Fig. 7 X-ray diffraction pattern of a mixture containing ch-BNs, PFOS, and Ca(OH)$_2$ after heating at 600 °C for 20 min. Conditions: [ch-BNs] = 0.5 g, [Ca(OH)$_2$] = 0.2 g, and [PFOS] = 0.2 g.

of several PFASs.[44,52] In this study, preliminary experiments were carried out to evaluate the stabilization performance of Ca(OH)$_2$ in the presence of ch-BNs. A mixture containing 0.5 g ch-BNs, 0.2 g Ca(OH)$_2$, and 0.2 g PFOS was calcined at 600 °C for 20 min. The resulting product was analyzed by X-ray diffractometer. The characterization results (Fig. 7) show that calcium fluoride (CaF$_2$) was produced during the calcination, providing solid evidence for the stabilization effectiveness of Ca(OH)$_2$ in the presence of BNs, which may suggest an approach to minimize gaseous PFAS emissions during the thermal regeneration of the BNs. The quantification with the TOPAS program (Fig. S4†) further showed that the product contained 0.1315 g CaF$_2$. Using eqn (5), the fluorine-fixing ratio was calculated to be 49.6%.

$$\text{Fluorine-fixing ratio} = \frac{2 \times \dfrac{\text{wt of CaF}_2}{\text{MW of CaF}_2}}{17 \times \dfrac{\text{wt of PFOS}}{\text{MW of PFOS}}} \times 100\% \quad (5)$$

4. Conclusions

In this study, graphene-like porous h-BNs were successfully synthesized and used as a sorbent to remove PFOS and PFDA from aqueous solution under different solution compositions. The h-BNs synthesized exhibited fast sorption for both PFOS and PFDA, reaching equilibrium within 2 h. The sorption processes fitted well with the pseudo-second-order kinetics and Freundlich model. Under conditions of 50 mg L^{-1} PFAS, 0.2 g L^{-1} h-BNs, and 5 mM ammonium acetate buffered pH 6.0, sorption amounts of ~0.72 mg m^{-2} and 0.45 mg m^{-2} were determined for PFDA and PFOS, respectively. The investigations on solution compositions show that H$^+$ and Ca^{2+} were influential, suggesting that the sorption processes were governed by the electrostatic force. The h-BNs regenerated via calcination showed good sorption stability and Ca(OH)$_2$, an additive during

calcination, was effective in the fixation of fluoride in the presence of BNs. On the basis of the above observations, we propose that h-BNs may be a promising material for the removal of PFASs from aqueous solutions. However, further studies are needed to investigate the uptake capacities of h-BNs toward other PFASs.

Conflict of interest

The authors declare no competing financial interest.

Acknowledgements

References

1 K. Prevedouros, I. T. Cousins, R. C. Buck and S. H. Korzeniowski, *Environ. Sci. Technol.*, 2005, **40**, 32–44.

2 A. G. Paul, K. C. Jones and A. J. Sweetman, *Environ. Sci. Technol.*, 2008, **43**, 386–392.

3 Z. Wang, I. T. Cousins, M. Scheringer, R. C. Buck and K. Hungerbühler, *Environ. Int.*, 2014, **70**, 62–75.

4 A. Jennifer, *J. Environ. Monit.*, 2003, **5**, 341–345.

5 A. Pistocchi and R. Loos, *Environ. Sci. Technol.*, 2009, **43**, 9237–9244.

6 R. Ma and K. Shih, *Environ. Pollut.*, 2010, **158**, 1354–1362.

7 B. C. Kelly, M. G. Ikonomou, J. D. Blair, B. Surridge, D. Hoover, R. Grace and F. A. P. C. Gobas, *Environ. Sci. Technol.*, 2009, **43**, 4037–4043.

8 K. H. Harada, H.-R. Yang, C.-S. Moon, N. N. Hung, T. Hitomi, K. Inoue, T. Niisoe, T. Watanabe, S. Kamiyama, K. Takenaka, M. Y. Kim, K. Watanabe, T. Takasuga and A. Koizumi, *Chemosphere*, 2010, **79**, 314–319.

9 H. Fromme, C. Mosch, M. Morovitz, I. Alba-Alejandre, S. Boehmer, M. Kiranoglu, F. Faber, I. Hannibal, O. Genzel-Boroviczény, B. Koletzko and W. Völkel, *Environ. Sci. Technol.*, 2010, **44**, 7123–7129.

10 J. P. Giesy and K. Kannan, *Environ. Sci. Technol.*, 2002, **36**, 146A–152A.

11 K. Kannan, S. H. Yun and T. J. Evans, *Environ. Sci. Technol.*, 2005, **39**, 9057–9063.

12 M. Clara, O. Gans, S. Weiss, D. Sanz-Escribano, S. Scharf and C. Scheffknecht, *Water Res.*, 2009, **43**, 4760–4768.

13 C. M. Butt, U. Berger, R. Bossi and G. T. Tomy, *Sci. Total Environ.*, 2010, **408**, 2936–2965.

14 A. K. Venkatesan and R. U. Halden, *J. Hazard. Mater.*, 2013, **252–253**, 413–418.

15 J. M. Maher, L. M. Aleksunes, M. Z. Dieter, Y. Tanaka, J. M. Peters, J. E. Manautou and C. D. Klaassen, *Toxicol. Sci.*, 2008, **106**, 319–328.

16 L. S. Kjeldsen and E. C. Bonefeld-jørgensen, *Environ. Sci. Pollut. Res. Int.*, 2013, **20**, 8031–8044.

17 H. Hori, E. Hayakawa, H. Einaga, S. Kutsuna, K. Koike, T. Ibusuki, H. Kiatagawa and R. Arakawa, *Environ. Sci. Technol.*, 2004, **38**, 6118–6124.

18 T. Yamamoto, Y. Noma, S. I. Sakai and Y. Shibata, *Environ. Sci. Technol.*, 2007, **41**, 5660–5665.

19 X. Li, P. Zhang, L. Jin, T. Shao, Z. Li and J. Cao, *Environ. Sci. Technol.*, 2012, **46**, 5528–5534.

20 H. Hori, A. Yamamoto, E. Hayakawa, S. Taniyasu, N. Yamashita, S. Kutsuna, H. Kiatagawa and R. Arakawa, *Environ. Sci. Technol.*, 2005, **39**, 2383–2388.

21 C. Liu, C. P. Higgins, F. Wang and K. Shih, *Sep. Purif. Technol.*, 2012, **91**, 46–51.

22 H. Moriwaki, Y. Takagi, M. Tanaka, K. Tsuruho, K. Okitsu and Y. Maeda, *Environ. Sci. Technol.*, 2005, **39**, 3388–3392.

23 J. Cheng, C. D. Vecitis, H. Park, B. T. Mader and M. R. Hoffmann, *Environ. Sci. Technol.*, 2008, **42**, 8057–8063.

24 J. Niu, H. Lin, C. Gong and X. Sun, *Environ. Sci. Technol.*, 2013, **47**, 14341–14349.

25 C. E. Schaefer, C. Andaya, A. Urtiaga, E. R. McKenzie and C. P. Higgins, *J. Hazard. Mater.*, 2015, **295**, 170–175.

26 J. C. Westall, H. Chen, W. Zhang and B. J. Brownawell, *Environ. Sci. Technol.*, 1999, **33**, 3110–3118.

27 C. P. Higgins and R. G. Luthy, *Environ. Sci. Technol.*, 2006, **40**, 7251–7256.

28 Q. Yu, R. Zhang, S. Deng, J. Huang and G. Yu, *Water Res.*, 2009, **43**, 1150–1158.

29 T. Yan, H. Chen, X. Wang and F. Jiang, *RSC Adv.*, 2013, **3**, 22480–22489.

30 Y. Wang, J. Niu, Y. Li, T. Zheng, Y. Xu and Y. Liu, *RSC Adv.*, 2015, **5**, 86927–86933.

31 R. L. Johnson, A. J. Anschutz, J. M. Smolen, M. F. Simcik and R. L. Penn, *J. Chem. Eng. Data*, 2007, **52**, 1165–1170.

32 C. Y. Tang, Q. S. Fu, D. Gao, C. S. Criddle and J. O. Leckie, *Water Res.*, 2010, **44**, 2654–2662.

33 F. Wang and K. Shih, *Water Res.*, 2011, **45**, 2925–2930.

34 X. F. Jiang, Q. Weng, X. B. Wang, X. Li, J. Zhang, D. Golberg and Y. Bando, *J. Mater. Sci. Technol.*, 2015, **31**, 589–598.

35 J. Li, X. Xiao, X. Xu, J. Lin, Y. Huang, Y. Xue, P. Jin, J. Zou and C. Tang, *Sci. Rep.*, 2013, **3**, 3208.

36 W. Lei, D. Portehault, D. Liu, S. Qin and Y. Chen, *Nat. Commun.*, 2013, **4**, 1777.

37 Y. Yu, H. Chen, Y. Liu, V. S. Craig, C. Wang, L. H. Li and Y. Chen, *Adv. Mater. Interfaces*, 2015, **2**, 1400267.

38 D. Liu, W. Lei, S. Qin and Y. Chen, *Sci. Rep.*, 2014, **4**, 4453.

39 J. Li, X. Xiao, X. Xu, J. Lin, Y. Huang, Y. Xue, P. Jin, J. Zou and C. Tang, *Sci. Rep.*, 2013, **3**, 3208.

40 F. Liu, J. Yu, X. Ji and M. Qian, *ACS Appl. Mater. Interfaces*, 2015, **7**, 1824–1832.

41 W. Lei, D. Portehault, D. Liu, S. Qin and Y. Chen, *Nat. Commun.*, 2013, **4**, 1777.

42 A. Nag, K. Raidongia, K. P. Hembram, R. Datta, U. V. Waghmare and C. Rao, *ACS Nano*, 2010, **4**, 1539–1544.

43 X. Lu, K. Shih and H. Cheng, *Water Res.*, 2013, **47**, 1353–1360.

44 F. Wang, K. Shih, X. Lu and C. Liu, *Environ. Sci. Technol.*, 2013, **47**, 2621–2627.

45 F. Wang, C. Liu and K. Shih, *Chemosphere*, 2012, **89**, 1009–1014.

46 Y. Ho and G. McKay, *Process Saf. Environ. Prot.*, 1998, **76**, 332–340.

47 Z. Piasek and T. Urbanski, *Bull. Pol. Acad. Sci., Tech. Sci.*, 1962, 113–120.

48 C. Huang, W. Ye, Q. Liu and X. Qiu, *ACS Appl. Mater. Interfaces*, 2014, **6**, 14469–14476.

49 Y. S. Ho and G. McKay, *Process Biochem.*, 1999, **34**, 451–465.

50 R. P. Schwarzenbach, P. M. Gschwend and D. M. Imboden, *Environmental organic chemistry*, John Wiley & Sons, 2005.

51 E. Kissa, *Fluorinated surfactants and repellents*, CRC Press, 2001.

52 F. Wang, X. Lu, X. y. Li and K. Shih, *Environ. Sci. Technol.*, 2015, **49**, 5672–5680.